IN-PLANE BEHAVIOUR OF POST-TENSIONED MASONRY WALLS

A. Mohamed A. ElGawady[1], B. Dongun Ryu [2] and C. Anil C. Wijeyewickrema [3]

[1] Associate Professor, Civil, Arch. and Environmental Eng. Dept., Missouri University S&T, 1401 N Pine St., Rolla, MO 65401. e-mail: elgawadym@mst.edu

[2] Graduate Research Assistant University of Tokyo, Former student Dept. of Civil and Environmental Engineering, Tokyo Institute of Technology, Tokyo, Japan

[3] Associate Professor, Dept. of Civil and Environmental Engineering, Tokyo Institute of Technology, Tokyo, Japan

ABSTRACT

In-plane behavior of unbonded post-tensioned clay brick masonry walls are investigated using detailed finite element (FE) models. Masonry is modeled as a homogenous isotropic material, the post-tensioning tendons are modeled using Hughes-Liu beam element. The material model is first calibrated using small scale prism tests available in the literature. Then, the finite element model is used to predict the cyclic behaviour of nearly full scale two post-tensioned masonry walls. The model correctly predicts the strength, stiffness, and stiffness degradation of the test specimens. The model is able to capture the rocking response of the specimens as well as the damage to the toes. The difference between the predicted and measured ultimate strength is within 7%. Furthermore, the model is able to correctly predict the variation in the post-tensioning force during the test.

KEYWORDS: finite element model, post-tensioning, shear walls, rocking

INTRODUCTION

Unreinforced masonry (URM) structures experienced severe damage due to moderate to strong earthquake ground motions. Several techniques have been investigated for retrofitting of URM walls [1-4]. Post-tensioning is another promising measure for retrofitting of URM structures. Vertical post-tensioning results in substantial improvement in the out-of-plane and in-plane strength and cracking load of URM walls. Post-tensioning is mainly used to retrofit structures characterized as monuments. This is due in part to lack of knowledge about the behavior of post-tensioned masonry walls. In addition, the codification of post-tensioned masonry has started recently [5-9].

Recently, research focuses on the application of post-tensioning technique for new masonry structures located in moderate to high seismic zones. To date, most construction applications of post-tensioned masonry have involved unbonded post-tensioning for its ease of construction and overall economy. An unbonded post-tensioned masonry wall (PT-MW) shows rocking behavior with large displacement when it is subjected to lateral loads. Furthermore, the self-centering behavior provided by the restoring force of the post-tensioning tendons reduces the residual displacement of PT-MWs. However, unbonded PT-MWs show low energy dissipation due to the lack of yielding of reinforcement. Adding mild steel at the base of PT-MW improves the energy dissipation and equivalent viscous damping but it increases the residual displacement of the wall [6, 10-14].

Wight [10] developed 3-D finite-element models to predict the in-plane strength of unbonded PT-MWs. The models were calibrated against the experimental results of five unbonded PT-MWs subjected to in-plane cyclic loading. However, those models failed in predicting the post-peak behavior of the walls. These 3-D models were used to carry out analyses of several walls and to develop an expression for tendon stress at ultimate state. Madan et al. [11] proposed finite element model to predict the flexural strength of unbonded post-tensioned concrete masonry walls under cyclic load.

Research on in-plane behavior of unbonded PT-MWs is limited. Rosenboom and Kowalsky [12] developed a simple force-displacement procedure that was able to predict the initial stiffness and peak strength of PT-MWs. However, it was not able to predict the ultimate displacement since degradation of masonry in the compressive zone and cyclic response of the tendons were not modeled.

The present study presents a detailed FE models for unbonded PT-MWs subjected to in-plane lateral cyclic loads. The material parameters of the numerical model are calibrated for masonry material characteristics using results of masonry prism tests reported by Ewing and Kowalsky (2004). To validate the numerical model, full scale masonry walls subjected to cyclic tests carried out by Rosenboom and Kowalsky [12] are used.

FINITE ELEMENT MODELING OF POST-TENSIONED MASONRY WALLS

Masonry is a composite material consisting of brick/block units, mortar, and grout. Researchers have modeled masonry walls using either discrete-crack (micro) or smeared-crack (macro) models depending on the required level of accuracy, availability of material properties, and resources for computations. Micro models are very time consuming and computationally demanding which makes it more appropriate for studying small masonry panels. Macro models are appropriate to study the behavior of large scale masonry walls where stresses across a macro-length are essentially uniform. Furthermore, it is computationally efficient, and hence, it is more practical [15].

In the present study, clay brick masonry is modeled as a homogenous isotropic material using a nonlinear material model. Finite element (FE) models of clay brick masonry walls are developed using LS-DYNA, an advanced general-purpose multi-physics simulation FE code. LS-DYNA is a well-known powerful FE simulation tool for solving highly nonlinear problems. It has several contact algorithms to simulate interaction between contact interfaces of discrete components which is an important feature for rocking structures [16].

Masonry is modeled using constant stress 8-node solid elements with one-point quadrature. Although this element has the advantage of less computer time due to one-point quadrature, the main disadvantage is that the element would result in spurious singular modes (i.e., hourglass modes). To overcome these spurious modes hourglass control procedures available in LS-DYNA are used. Karagozian and Case (K& C) material model, implemented as MAT_CONCRETE_DAMAGE_REL3 (MAT_072R3) is one of the available models in LS-DYNA that can be used for masonry by calibrating model parameters to masonry material characteristics [17]. The K&C material model uses a three-surface plasticity formulation where shear failure surfaces, viz. yield, maximum, and residual are defined for deviatoric response of

the material [18-19]. To define these surfaces, the model has material parameter generation capability associated with the compressive strength of the specified material. However, these parameters have to be calibrated using data from material testing of masonry prisms. The volumetric response of the material is governed by a multi-linear compaction model and values used to define pressure versus volumetric strain response are assigned using equation-of-state EOS_TABULATED_COMPACTION model. The pressures and unloading bulk moduli are calculated for given strains using relations given by Crawford and Malvar (2006) where the bulk modulus K for masonry is given by,

$$K = \frac{E}{3(1-2\upsilon)} \tag{1}$$

where Poisson's ratio ν = 0.2 and elastic modulus E= 700f'$_m$ in which f'$_m$ is compressive strength of masonry [20].

The post-tensioning tendon and horizontal reinforcement are modeled using Hughes-Liu beam element with 2×2 Gauss quadrature. The material model MAT_PLASTIC_KINEMATIC (MAT_003) is used to model both the post-tensioning tendons and shear reinforcement. This model can be used for isotropic, kinematic or a combination of isotropic and kinematic hardening, and in the present study, kinematic hardening is used for the tendons. The material properties of the tendons are density 8000 kg/m3 (499 lb/ft3), Young's modulus 205 GPa (29700 ksi), Poisson's ratio 0.3, yield stress 890 MPa (129ksi), and tangent modulus 3.1 GPa (450 ksi). The material properties used for the shear reinforcement are density 8000 kg/m3 (499 lb/ft3), Young's modulus 200 GPa (29000 ksi), Poisson's ratio 0.3, yield stress 420 MPa (60.9 ksi), and tangent modulus 1.5 GPa (217 ksi).

CALIBRATION OF THE MATERIAL MODEL

To obtain the material parameters that would simulate the full-scale masonry walls, the K&C material model is first calibrated using small scale prism tests available in the literature. Ewing [14] considered grouted double-wythe masonry prisms subjected to axial load in displacement control and the stress-strain characteristics of those specimens were investigated (Fig. 1a). Fig. 1(b) shows the FE model used in the present study for masonry prism testing. The load is applied to the top of the prism in displacement control similar to the experiment. The three translational U_x, U_Y, and U_Z degrees of freedom are constrained for all the nodes at the bottom surface of the masonry prism. Fig. 2 shows the stress-strain curves obtained from numerical analysis and the experiment for axial load test of the prism. The investigated prism has a peak stress f'$_m$ of 25.9 MPa (3.8 ksi) and an axial strain at peak stress of 0.0017. For post-peak behavior (i.e., during softening), the axial strain values corresponding to 0.5 f'$_m$ and 0.2 f'$_m$ are 0.005 and 0.0087, respectively. As shown in the figure the stress-strain behavior obtained from the calibrated K&C model closely correlates with those measured in the experiment.

VALIDATION OF THE FE MODEL USING FULL-SCALE TESTS

Two walls are used for validation of the FE model. The first wall (hereafter called W1) was tested by [12] and shown in Fig. 3(a). The wall has length, height, and width of 1.2 m (3.9 ft), 2.135 m (7.0 ft), and 0.305 m (1 ft.), respectively. The wall was post-tensioned using three vertical tendons at a horizontal spacing of 458 mm (1.5 ft.) corresponding to 1.5 times the wall

nominal thickness (1.5t). The post-tensioning was applied using 25.4 mm (1 in.) diameter Dywidag high-strength threaded bars. Each bar was installed in a 38 mm (1.25 in.) internal diameter PVC duct. Each post-tensioning bar was post-tensioned to 333 kN (74.9 Kips), which is about two-third of its ultimate strength, with a total post-tensioning force of approximately 1000 kN (224.8 Kips).

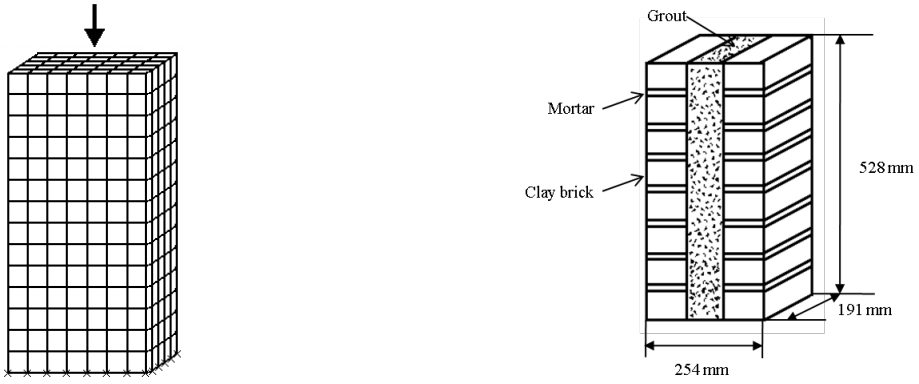

(a) (b)

Figure 1: Grouted Double-Wythe Masonry: a) Prism Used in Experiment (Ewing and Kowalsky 2004), and b) Finite Element Model Used for the Calibration of Material Parameters of the Numerical Model

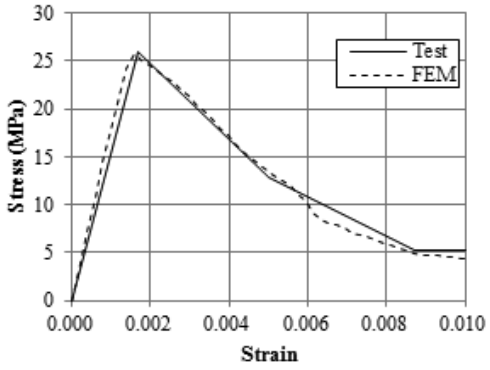

Figure 2: Comparison between Measured and Computed Stress-Strain Behavior of Double Wythe Prism under an Axial Load

The second wall (hereafter called W2) was tested by Ewing [13]. It has length, height, and width of 2.3 m (7.5 ft), 2.2 m (7.2 ft), and 0.3 m (1 ft), respectively. The wall W2 has an opening having a length of 0.9 m (3.3 ft) and height of 1.5 m (4.9 ft). The opening was centered with respect to a vertical axis passing through the middle of the wall. The wall was post-tensioned using four high strength Dywidag 15.9 mm (0.63 in.) diameter bars where two bars were in each pier. The bars were placed inside PVC tubes 300 mm (1 ft.) apart and centered within each pier. This spacing corresponding to one times the wall nominal thickness (i.e., 1.0t). Each bar was

subjected to 60 kN (13.49 kips) of post-tensioning force which was about one-third of its ultimate strength.

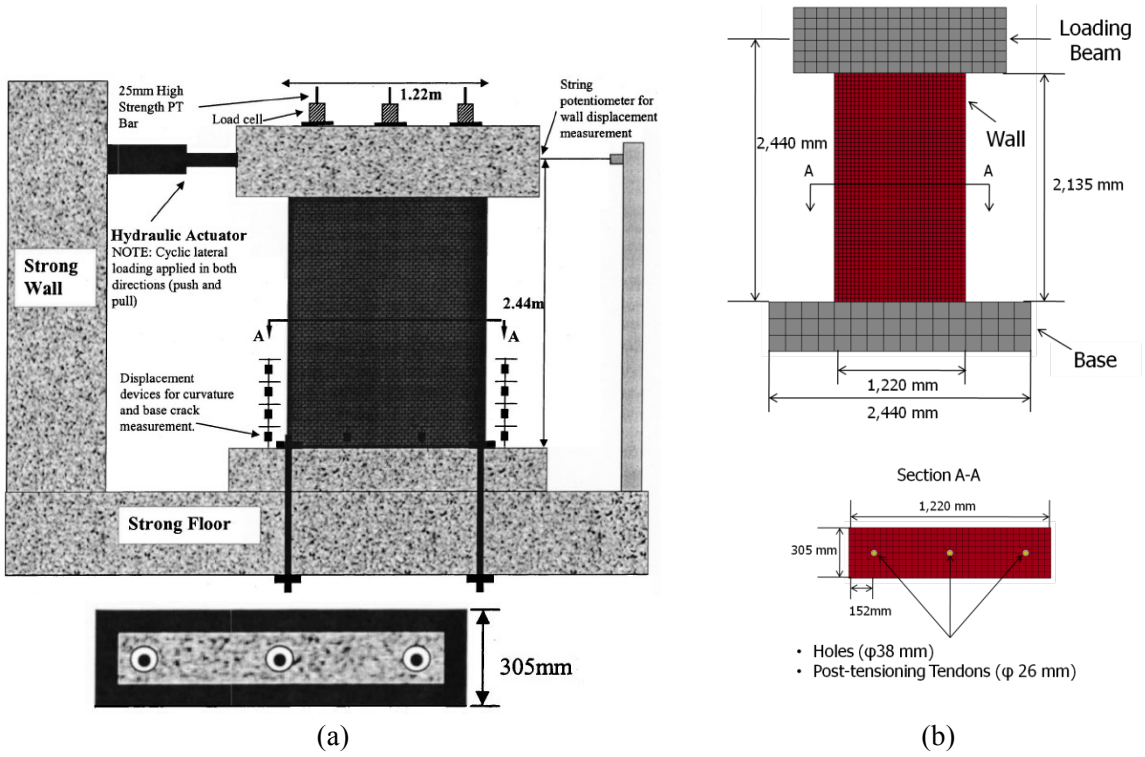

(a) (b)

Figure 3: Wall W1 a) Test Setup (Rosenboom and Kowalsky 2004), and b) Details of the Finite Element Model.

Each wall was built on a reinforced concrete foundation, which was fixed to the laboratory strong floor, and was free to rotate at the top of the wall that can be idealized as a cantilever wall. The walls were subjected to in-plane cyclic loading of increasing amplitude.

Fig. 3(b) shows the FE model of wall W1 which consists of 19,901 nodes and 16,196 elements. Cap-beam, masonry wall, and concrete base are modeled using solid elements. A fine mesh is used for the masonry wall; the average element size is 46 mm (1.8 in.). Sensitivity analysis was carried out to determine the element size that resulted in good compromise between accuracy and computational efforts. For the loading beam and the base, a coarse mesh is used since the deformations of the loading beam and the base are negligible.

Masonry is modeled as homogenous material using the K&C material model. The cap-beam and base footing are modeled using elastic materials. Vertical holes where the tendons would be placed are created in the wall. The contact between the masonry wall and the reinforced concrete (RC) foundation as well as between the masonry wall and the RC cap-beam is defined using the contact type CONTACT_AUTOMATIC_SURFACE_TO_SURFACE allowing the interface joint to be opened under tensile forces i.e. ignoring mortar tensile strength. Furthermore, this contact allows for compressive forces to be transformed between the contact

surfaces. The shear forces between masonry and concrete (either cap-beam or foundation) are transmitted using the Coulomb friction with a coefficient of friction of 0.5.

The post-tensioning tendons in the model are embedded at the top into the cap-beam and at the bottom into the foundation (Fig. 3b). The contact behavior between the masonry surface and the tendon is modeled using the contact type CONTACT_AUTOMATIC_NODE_TO_SURFACE. Two loading steps are used for the analysis of the models. First, gravity load is applied to the loading beam as a body force load in the vertical direction. Then, a post-tensioning force is applied to the post-tensioning tendons using the option INITIAL_STRESS_BEAM. Second, the lateral load is applied to the cap-beam. During the experimental work, both Walls W1 and W2 were tested using a displacement-based protocol consisting of three cycles at each peak displacement value. During the numerical analysis, each wall was subjected to similar loading pattern but with one cycle at each peak displacement. Moreover, another set of analysis of the walls was carried out using pushover analysis. In the pushover analysis, the wall was subjected to lateral displacement of increasing amplitude until failure occurred.

The FE model of the wall W2 consists of 27,894 nodes and 22,764 elements. Similar to the wall W1, the loading beam, the wall and the base are modeled using solid element, the post-tensioned tendons were modeled using beam element, and masonry is modeled as a homogenous material using solid element. Contact algorithms similar to those described before for the wall W1 are used. Sliding and rocking are allowed to take place between the wall and its foundation, masonry piers and their spandrel, masonry piers and the cap-beam (Fig. 4).

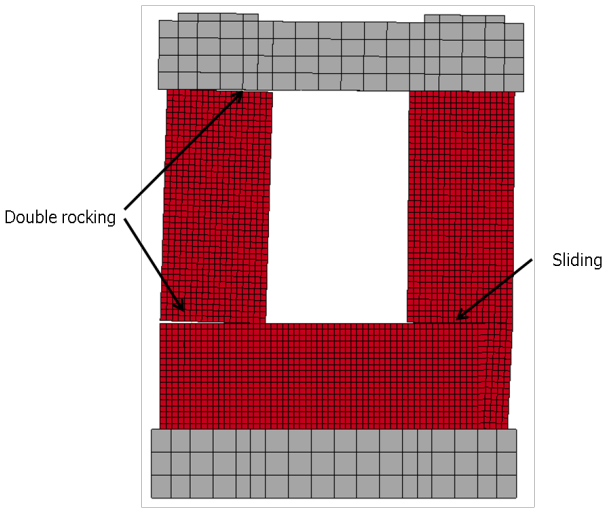

Figure 4: The Finite Element Model Showing Rocking and Sliding of Specimen W2

RESULTS OF THE VALIDATION OF FULL-SCALE WALLS

Fig. 5 shows comparisons between the hysteretic response of the test specimen [12] and that obtained from the FE analysis. The backbone curves obtained from both experiment and the pushover analysis are shown in Fig. 6. Fig. 7 shows the damage pattern to wall W1 observed in the test and the one obtained using the FE analysis. During the test, the first crack appeared at a drift of 0.2% at the base of the wall followed by vertical splitting crack occurred in the toe at a drift of 1.25%. The wall reached its peak strength of 330 kN (74.2 kips) at drift of 1.75%.

Strength degradation started at a drift of 3% and the test was stopped at drift of 6.5% where the wall toes, extending about 200 mm (0.66 ft) from the wall edges, significantly damaged as shown in Fig. 7(a).

The FE model is able to closely simulate the behavior observed in the test (Figs. 5-8). Both the FE analysis and test shows similar symmetrical response. As shown in Figs. 5 and 6, the estimated peak forces, ultimate displacement, stiffness degradation, and hysteretic pinching agree well with the experiment results. The maximum lateral force obtained using FE analysis is 326 kN (73.3 kips) compared to 330 kN (74.2 kips) measured during the test. Similarly, the ultimate displacement of approximately 145 mm (0.48 ft) obtained using the FE analysis is very close to the one measured during the test. The initial stiffness obtained using the FE analysis agrees well with the measured initial stiffness. Damage to the wall confines to the toe regions of the wall; similar to what was observed during the test (Fig. 7b).

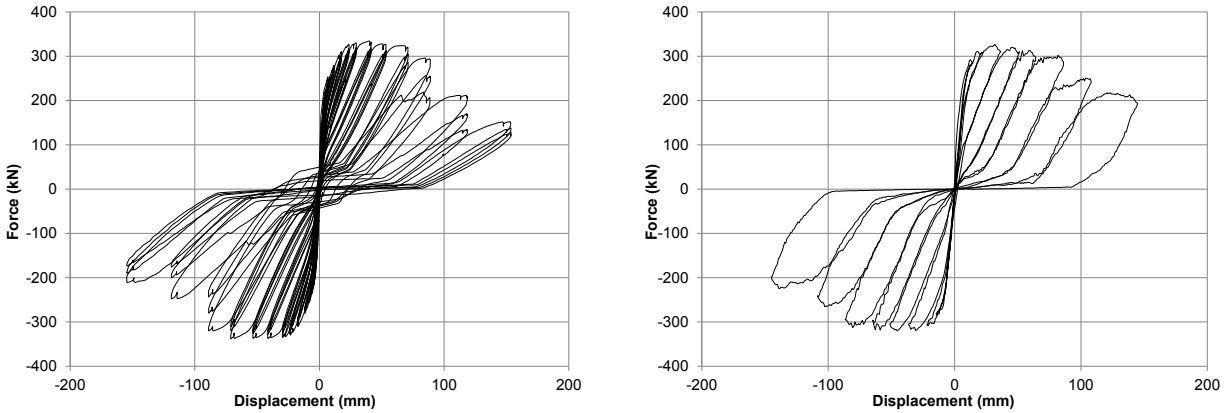

(a) (b)

Figure 5: Force-displacement history of wall W1: a) experiment (Rosenboom and Kowalsky 2004) and b) numerical analysis

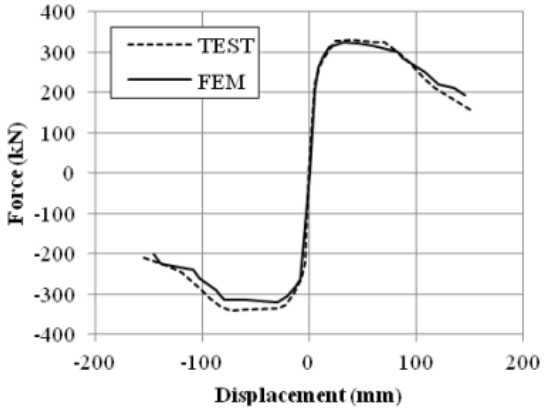

Figure 6: Comparison of Backbone Curves for Wall W1 Obtained from Experiment and Numerical Analysis

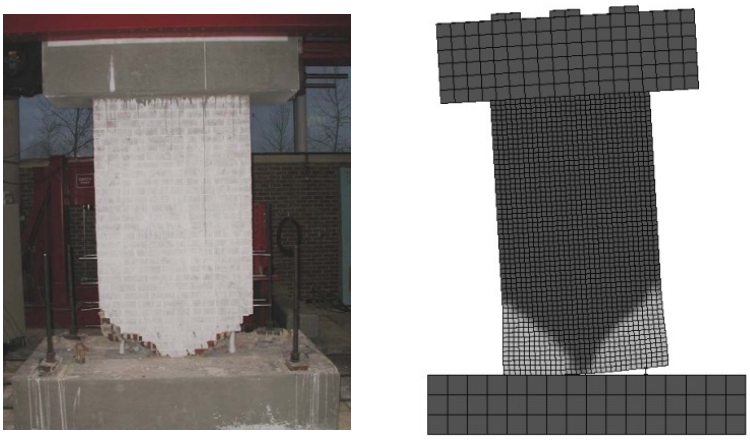

Figure 7: Comparison of Damage Pattern of Wall W1: a) Experiment (Rosenboom and Kowalsky 2004) and b) Numerical Results Showing Damage Contours

As shown in Fig. 8, during cyclic behavior of the wall, the total post-tensioning force in the wall varied significantly and reached a maximum value of approximately 1200 MPa (174 ksi). Fig. 8(b) shows the change in the total post-tensioning force in the three tendons versus the applied lateral displacement. This variation in the total post-tensioning force is correctly captured by the FE model. The total post-tensioning force at any loading cycle agrees well with those measured during the test and it varies between 800 kN (179.8 kips) to 1200 kN (269.8 kips). However, during unloading, the FE model underestimates the total post-tensioning forces.

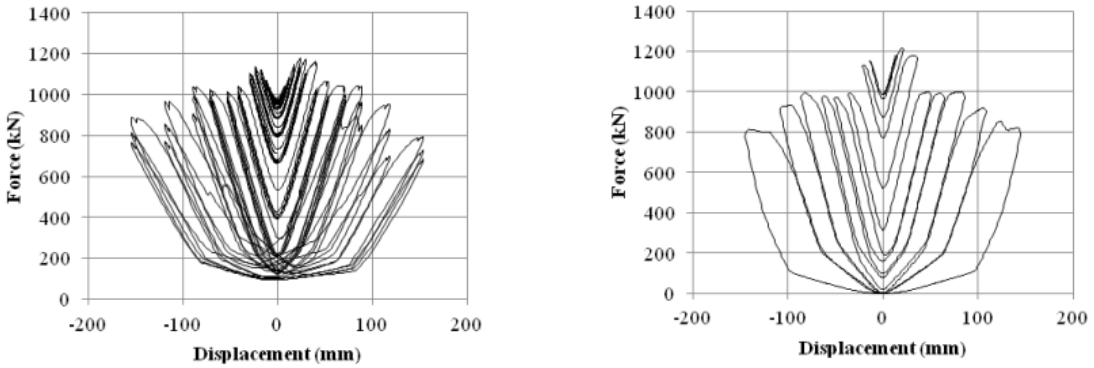

Figure 8: Total Prestressing Force History of Wall W1: (a) Experiment (Rosenboom and Kowalsky 2004) and (b) Numerical Analysis.

For wall W2, both the FE analysis and experiment shows rocking behavior at drift of 0.25% at two interface joints: one at the top of the spandrel beam and the second one above the piers i.e., below the cap-beam. At a drift of 0.35%, a vertical splitting crack extending across the bottom spandrel beam occurred in the experiment (Fig. 9a). At the same drift, the FE model shows a high stress concentration at the splitting crack location (Fig. 9b). The rocking behavior of the wall continued, and it combined with sliding of the piers and the test was ended at a drift of 2.25%. The FE analysis shows a sliding displacement of approximately 15 mm (0.6in.) compared to the measured 18 mm (0.71) in the test. One difference between the test and the FE

analysis is that in the test the sliding plane was asymmetric while the FE model shows a symmetric sliding plane (Figs. 9-10).

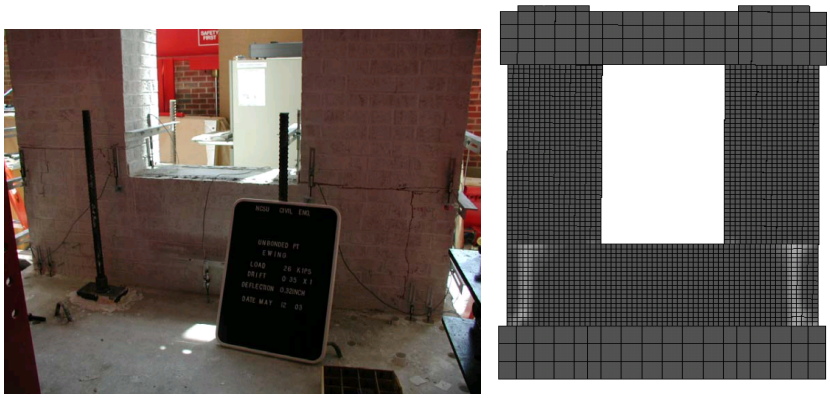

(a) (b)

Figure 9: Comparison of Damage Pattern of Wall W2 at Drift of 0.35%: (a) Experiment (Ewing 2008) and (b) Numerical Results Showing Regions of High Stress Concentration

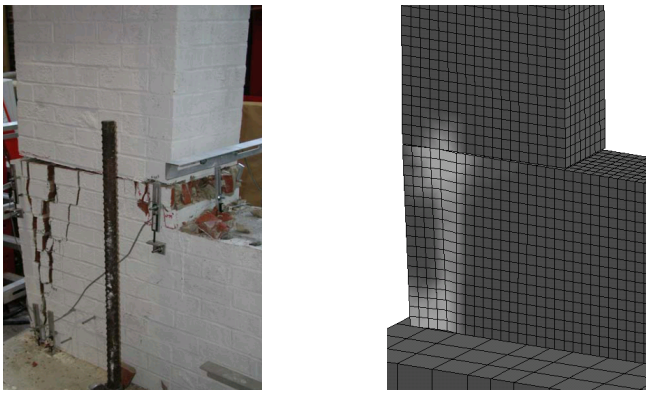

(a) (b)

Figure 10: Comparison of Damage Pattern of Wall W2 at Drift of 2%: (a) Experiment (Ewing 2008) and (b) Numerical Results Showing a Region of High Stress Concentration

The test showed that sliding took place at the second brick course above the spandrel in one direction and between the spandrel and the pier in the other direction. The FE model shows a symmetric response with sliding took place just above the spandrel. This asymmetric response in the test may be associated with some local anomalous during the construction process. The results of the FE under cyclic and pushover loading showed that the models are able to accurately simulate the hysteretic response and backbone curves of the experiment (Figs. 11 and 12), respectively. As shown in Fig. 12, the peak force measured during the test is 7% higher than the one obtained from the FE analysis. Furthermore, the initial stiffness and ultimate displacement also agree well with the experimental results.

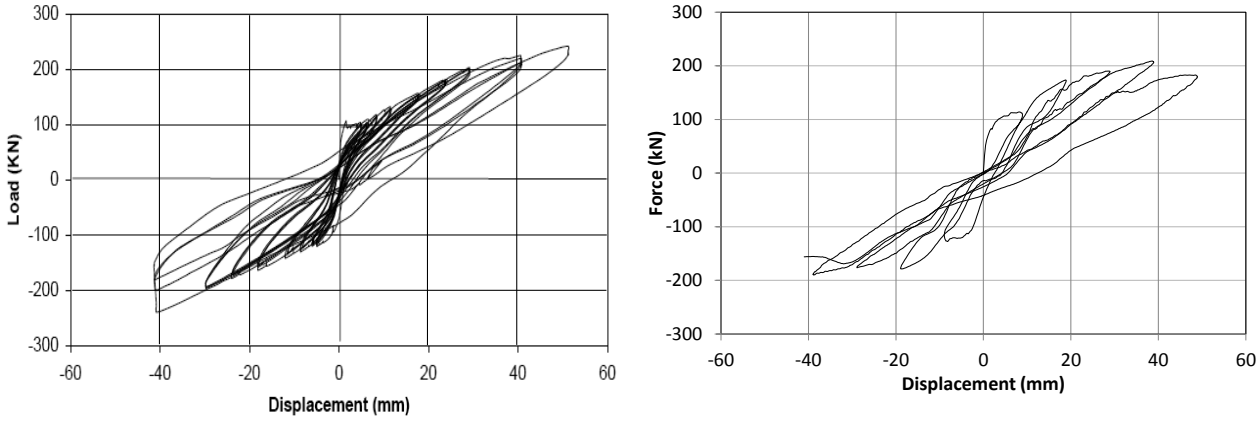

(a) (b)

Figure 11: Force-displacement history of wall W2: (a) experiment (Ewing 2008) and (b) numerical analysis

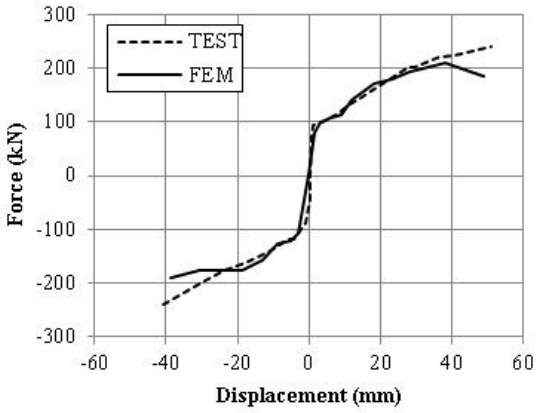

Figure 12: Comparison of Backbone Curves for Wall W2 Obtained from Experiment and Numerical Analysis

SUMMARY

In the present study, in-plane behavior of unbonded post-tensioned clay brick masonry walls are investigated using detailed finite element models. Experimental results available in the literature are used to calibrate the material parameters of the numerical model for masonry material characteristics using results of prism tests. To validate the numerical model experimental results of full scale masonry walls are considered.

ACKNOWLEDGMENT

The authors would like to thank Prof. Mervyn Kowalsky (North Carolina State University) for providing the experimental data used in the validation of the finite element model.

REFERENCES

1. Abrams, D. P., and Lynch, J. M. (2001). “Flexural behavior of retrofitted masonry piers.” KEERC-MAE Joint Seminar on Risk Mitigation for Regions of Moderate Seismicity, IL
2. ElGawady, M. A., Lestuzzi, P., and Badoux, M. (2006). “Analytical model for the in-plane shear behavior of URM walls retrofitted with FRP.” Comp. Science Tech., 66 (3-4), 459-474.
3. Taghdi, M. (2000). “Seismic retrofit of low-rise masonry and concrete walls by steel strips.” Ph.D. dissertation, Department of Civil Engineering, University of Ottawa, Ottawa, Canada.
4. Rai D., and Goel, S. (1996). “Seismic strengthening of unreinforced masonry piers with steel elements.” Earthquake Spectra, 12, 845-862.
5. Schultz, A. E., and Scolforo, M. J. (1991). "An Overview of Prestressed Masonry," TMS Journal, The Masonry Society, 10(1), 6-21.
6. Schultz, A., Bean, J., Stolarski, H. (2003). ‘‘Resistance of slender post-tensioned masonry walls with unbonded tendons to transversal loading.’’ Proceedings 9NAMC, Clemson, SC, 463-473.
7. Lissel, S. L., and Shrive, N. G. (2003). “Construction of diaphragm walls post-tensioned with carbon fiber reinforced polymer tendons.” Proceedings 9NAMC, Clemson, SC, 192-203.
8. Bean, J. R., and Schultz, A. E. (2003). “Flexural capacity of post-tensioned masonry walls: Code review and recommended procedure.” PTI J., 1(1), 28-44.
9. Bean Popehn, J.R. and Schultz, A.E. (2010) "Design Provisions for Post-Tensioned Masonry Walls Loaded Out-of-Plane," TMS Journal, The Masonry Society, 28(2):9-26.
10. Wight, G. (2006). “Seismic Performance of a Post-tensioned Concrete Masonry Wall System.” Ph.D. dissertation, Dept. Civil Eng., University of Auckland, New Zealand.
11. Madan, A., Reinhorn, A. M., and Mander, J. B. (2008). “Fiber-Element Model of Posttensioned Hollow Block Masonry Shear Walls under Reversed Cyclic Lateral Loading.” J. Struct. Eng., 134(7), 1101-1114.
12. Rosenboom, O. A., and Kowalsky, M. J. (2004). “Reversed In-Plane Cyclic Behavior of Post-tensioned Clay Brick Masonry Walls.” J. Struct. Eng., 130(5), 787-798.
13. Laursen, P. T. (2002). “Seismic analysis and design of post-tensioned concrete masonry walls.” Ph.D. dissertation, Dept. Civil Eng., University of Auckland, New Zealand.
14. Ewing, B. D. (2008). “Performance of Post-Tensioned Clay Brick Masonry Walls with Openings.” PhD dissertation, NC State University, Civil Engineering, Raleigh, NC, USA.
15. El-Dakhakhni, W. W., Elgaaly, M., and Hamid, A. A. (2003). “Three-strut model for concrete masonry-infilled steel frames.” J. Struct. Eng., 129(2), 177-185.
16. LS-DYNA. (2007). “Keyword user’s manual.” Livermore Software Technology Corporation, CA.
17. Magallanes, J. M. (2008). “Importance of concrete material characterization and modelling to predicting the response of structures to shock and impact loading.” Structures Under Shock and Impact X, 98, 241-250.
18. Crawford, J. E., and Malvar, L. J. (2006). “User’s and theoretical manual for K&C concrete model.” Report TR-06-19.1, Karagozian & Case, CA, USA.
19. Malvar, L., Crawford, J., Wesevich, J., and Simons, D. (1997). “A plasticity concrete material model for DYNA3D.” Int. J. Impact Eng., 19(9–10), 847–873.
20. MSJC (2008). “Building code requirements and specifications for masonry structures.” ACI 530-05/ASCE 5-05/TMS 402-05, Masonry Standards Joint Committee, Amer. Conc. Ins.